I/Q Demodulator Based Optical Camera Communications

Hiroaki Matsunaga, *Student Member, IEEE*, Tomohiro Yendo, Wataru Kihara, Yoshifumi Shiraki, *Member, IEEE*, Takashi G. Sato, *Member, IEEE*, and Takehiro Moriya, *Life Fellow, IEEE*

***Abstract*—Visible light communications achieve wireless communications using light sources such as lighting fixtures and electric signboards. The light sources need to blink at high speed to avoid flickering. However, the blinking frequency is much higher than the frame rate of the general-purpose cameras that are integrated into consumer devices such as smartphones. This paper proposes a method where the principle of the I/Q demodulator as employed in radio frequency communications is used to estimate the phase and amplitude of modulated light blinking at a sufficiently higher speed than the frame rate. This is achieved by using two cameras with slightly different exposure start timing and estimating the phase and amplitude from the pixel values of the light-emitting diode (LED) image in one frame for each camera. In contrast to the conventional method with a very short exposure time, the exposure time can be increased, resulting in higher efficiency of light capture. Additionally, we propose another configuration employing one camera and two LEDs. An experiment to verify that communication is possible with the proposed method, which achieved 200 bits/s with 60 frames per second cameras. We also confirmed the proposed methods have similar signal-to-noise ratio to bit error ratio performance.**

***Index Terms*—I/Q demodulator, non-flickering communications, optical camera communication (OCC), visible light communications (VLC).**

I. Introduction

LIGHT-emitting diodes (LEDs) are being utilized in an increasing number due to their advantages of high energy efficiency, long lifespan, low hazardous material usage, and small size [1], [2]. Due to the fast response time of LEDs, the use of LED light as a medium for wireless communications has been studied [3]. This optical wireless communications technology is called visible light communications (VLC) [4], where the blinking of the light source is modulated for data transmission. The advantages of VLC are that electromagnetic interference can be avoided and communications without a license is possible in many countries.

VLC uses photodiodes (PDs) or cameras as receivers [2] to capture the transmitted light signal. PD-based methods can achieve high-speed communications of up to several gigabits per second [5]; however, light from sources other than the target transmitter, such as ambient light or light from other transmitters can interfere with the signal transmission. On the other hand, camera-based methods suppress the influence of ambient light and can capture light from each source independently. This is because the optics of the camera projects the light to different positions on the image sensor depending on the direction of the incoming light. Camera-based communications methods are collectively called optical camera communications (OCC). By using high-speed cameras, communications speeds of tens of kilobits per second can be achieved, although they are inferior to those of PD-based methods [6], [7]. However, high-speed cameras are expensive and are not widely used. On the other hand, methods have been proposed about utilizing the widely used general-purpose cameras embedded in mobile devices such as smartphones [8]. Although the communication speed is limited, this approach is expected to significantly reduce the cost of installing receivers for users.

One of the important applications of OCC is the integration of communication functions into appliances such as lighting fixtures and electronic billboards. In these applications, flicker must not be perceived by the human eye. The lower frequency limit of flicker-free blinking is considered to be about 100 Hz [9]. However, general-purpose cameras have a limited frame rate, which is about 60 frames per second (fps) [8]. Methods using the rolling shutter effect [10]–[13] and undersampling methods have been studied extensively [14]–[20] as ways to capture and receive data from fast-blinking light sources with general-purpose cameras.

The rolling shutter effect can provide a sampling rate that is much higher than the frame rate, and hence signals such as on-off keying (OOK) above 100 Hz can be sampled directly, and the communication speed is higher than the under-sampling method. However, the light from one transmitter light source has to be received by many pixel lines of the image sensor, which limits the communication distance [8] and makes it difficult to separate light from multiple transmitters.

Manuscript received February 8, 2022; revised March 25, 2022; accepted April 4, 2022. Date of publication April 11, 2022; date of current version April 28, 2022. *(Corresponding author: Hiroaki Matsunaga.)*

Hiroaki Matsunaga is with the Information Science and Control Engineering, Nagaoka University of Technology, Niigata 940-2188, Japan (e-mail: s163211@stn.nagaokaut.ac.jp).

Tomohiro Yendo and Wataru Kihara are with the Electrical, Electronics and Information Engineering, Nagaoka University of Technology, Niigata 940-2188, Japan (e-mail: yendo@vos.nagaokaut.ac.jp; banana0re1@gmail.com).

Yoshifumi Shiraki, Takashi G. Sato, and Takehiro Moriya are with the Nippon Telegraph and Telephone Corporation, Kanagawa 2430198, Japan (e-mail: yoshifumi.shiraki.ya@hco.ntt.co.jp; takashi_goto_sato@ieee.org; t.moriya@m.ieice.org).

Digital Object Identifier 10.1109/JPHOT.2022.3166283

In contrast, undersampling methods use one sample value, which is equal to a single pixel value or a sum of multiple pixel values per LED in one frame and demodulates it and can thus achieve long-range and multichannel communications. In this approach, the light source blinks at a frequency higher than the sampling rate, so a method to detect the change of statuses such as phase, amplitude, or frequency of the blinking light source is necessary. One strategy for this purpose is to employ a very short exposure time on a camera and capture changes in blinking status, such as changes in phase, amplitude, and frequency. However, short-exposure undersampling has low efficiency in capturing light energy due to the very short exposure time of around $1/2000$ s, and the phase that can be used for symbols is limited to binary values. Methods have been proposed to make the exposure time longer. One, UPFSOOK [14], has achieved 160 m communications, and another, SW-QAM [21], allows multilevel modulation by phase and amplitude. However, UPFSOOK does not use multilevel symbols, and SW-QAM requires three frame sample values to estimate the phase and amplitude. The efficiency of these methods has room for improvement.

In this paper, as a new undersampling method, we propose a communications method where an I/Q demodulator uses sample values to estimate the blinking phase and amplitude in multiple levels. I/Q demodulators are widely used in radio frequency (RF) communications, where they extract the phase and amplitude from modulated RF waves without sampling them directly [22]. The proposed method exploits a demodulation mechanism with two cameras that work like an I/Q demodulator. The proposed method extracts the information in two-dimensional multilevel phase and amplitude modulation from two sample values (two-dimensional) captured by longer exposure time. Thus, it achieves higher transmission efficiency in terms of power consumption or the amount of information per sample value than most previous methods. In addition to a simple implementation of the proposed method with two cameras and one LED, a configuration with one camera and two LEDs is also available. This variation enables flexible system configuration. Note that the proposed method obtains one pixel value for one LED in one frame, and focuses on the changes in pixel values with respect to time.

The contributions of this paper are as follows. By using the principle of the I/Q demodulator in OCC, it is possible to extract the blinking phase and amplitude as continuous values from two sample values which are obtained by two cameras with a speed slower than the LED blinking frequency. In addition, we have achieved communications with a longer exposure time compared to conventional methods that employ a very short exposure time. Furthermore, this method can be implemented in two configurations—two cameras with one LED, and one camera with a pair of LEDs—which can be employed according to requirements under different conditions. We have shown that the use of a square wave carrier signal in the proposed method results in different properties compared to those of the conventional I/Q demodulator. An experiment with the proposed method has shown the signal-to-noise ratio to bit error ratio (SNR-BER) characteristics for multilevel PSK and QAM for both the two camera and two LED methods.

The remainder of this paper is organized as follows: Section II introduces related work. Section III describes the principle of the proposed method and the problems and solutions in using it for communications. Section IV describes the experiments to verify the communication; Section V discusses the experimental results, and Section VI concludes the paper with a brief summary. Note that this work is an expansion of our conference papers [23], [24].

II. Related Work

For achieving flicker-free communications with a general-purpose camera as a receiver, it is necessary to capture changes in the high-speed blinking status. To avoid the flicker, the blinking frequency of the light source must be above 100 Hz [9], and 200 Hz or higher is recommended [25]. To perform flicker-free OCC reception on devices such as smartphones embedded with cameras with a frame rate of about 60 fps, one should introduce methods that enable them to capture changes in this high-speed LED blinking. Flicker-free OCC methods using a general-purpose camera with a fast-blinking light source can be broadly classified as those based on the rolling shutter effect and undersampling [26].

Rolling-shutter-based methods sample high-speed waveforms using a general-purpose camera by exploiting the rolling shutter phenomenon, where slight differences in the exposure timing of each line of pixels occur in complementary metal-oxide-semiconductor (CMOS) image sensors [10]–[13]. This technique can achieve transmission speeds of a few kilobits per second or more. However, there are limitations on transmission distance and the size of the light source because the captured image is too small and the rolling shutter phenomenon cannot be exploited when there are only a few pixel lines on the image sensor to receive the light.

On the other hand, undersampling methods estimate the blinking change based on the value of one sample per frame and one LED. Unlike the rolling shutter method, they can effectively utilize the spatial separation by camera optics, which is an advantage of OCC. Many under-sampling methods use extremely short exposure times to extract changes in phase, amplitude, and frequency by sampling at a frequency that is a fraction of the blinking frequency [15]–[20]. These short-exposure undersampling methods have been widely studied. However, they are less efficient in capturing light due to the short exposure time. Moreover, they can only detect binary phase differences, and the order of multilevel modulation depends on the amplitude order. This limits the design of the transmitter. A method with a longer exposure time has achieved long-distance communications of 160 m [14]. The modulation in this method utilizes frequency, and the employed symbol is only binary. Another type of undersampling method with longer exposure time, SW-QAM [21], allows multilevel modulation by phase and amplitude. However, this method requires three values to extract two dimensions of information, i.e., the phase and amplitude, and thus does not efficiently utilize the information of sample values.

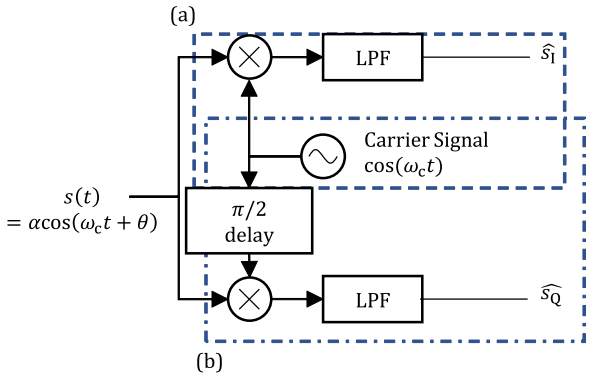

Fig. 1. I/Q demodulator in radio communication. $\widehat{s_I}$ is the demodulated in-phase component, and $\widehat{s_Q}$ is the demodulated quadrature component. (a) In-phase component demodulator part; (b) quadrature component demodulator part.

In this paper, as a type of under-sampling method, we propose a technique that estimates the phase and amplitude using two cameras with different exposure start timing by applying the principle of the I/Q demodulator used in RF communications. This method enables flexible transmitter and receiver design with the use of multiple values of phase in addition to amplitude. Since the exposure time is set to half of the blinking period, it can be longer than that in existing short-exposure under-sampling methods. It is also more efficient than SW-QAM as it extracts two-dimensional multilevel information (phase and amplitude) from two sample values.

III. Proposed Communication Method

A. Implementation of I/Q Demodulation Principle for OCC

To obtain the phase and amplitude of a LED blinking at a high frequency above the normal frame rate on a general-purpose camera, we employ the I/Q demodulator mechanism instead of capturing the blinking waveform directly. Generally, in radio communications, parameters of a carrier wave such as its frequency, phase, and amplitude are varied according to the symbol, which is the smallest unit of communication, and these parameters are retrieved by a receiver. An I/Q demodulator is commonly used in RF communications to obtain the phase and amplitude of high-frequency received signals without having to directly observe the high-speed waveform [27], [28]. The structure of the demodulator is shown in Fig. 1. By using an I/Q demodulator, baseband signals corresponding to phase and amplitude whose frequency is much lower than that of carrier wave are obtained.

The principle of the I/Q demodulator is explained as follows. The amplitude of the modulated RF wave $s(t)$ is α, and its phase is advanced by θ from the carrier signal $\cos(\omega_c t)$, where ω_c is the angular frequency. By using in-phase component s_I and quadrature component s_Q, which are expressed with phase θ $(0 \leq \theta < 2\pi)$ and amplitude α $(0 \leq \alpha \leq 1)$ as

$$s_I = \alpha\cos(\theta), \quad s_Q = \alpha\sin(\theta), \tag{1}$$

s(t) can be computed as

$$s(t) = \alpha\cos(\omega_c t + \theta) = s_I\cos(\omega_c t) - s_Q\sin(\omega_c t). \tag{2}$$

In the I/Q demodulator, the input $s(t)$ is multiplied by the in-phase local carrier $\cos(\omega_c t)$ as

$$s(t)\cos(\omega_c t) = \frac{s_I}{2} + \frac{s_I}{2}\cos(2\omega_c t) - \frac{s_Q}{2}\sin(2\omega_c t). \tag{3}$$

The input $s(t)$ is also multiplied by the quadrature local carrier $-\sin(\omega_c t)$ which has $\pi/2$ delay from the in-phase local carrier, as

$$-s(t)\sin(\omega_c t) = \frac{s_Q}{2} - \frac{s_Q}{2}\cos(2\omega_c t) - \frac{s_I}{2}\sin(2\omega_c t). \tag{4}$$

After the high-frequency components from signals $s(t)\cos(\omega_c t)$ and $-s(t)\sin(\omega_c t)$ are removed by a low-pass filter (LPF), the demodulated in-phase component $\widehat{s_I}$ and quadrature component $\widehat{s_Q}$ are obtained, respectively.

In the proposed method principle, this demodulator configuration is used in OCC. Since the relationship between the light incident on the camera and the pixel value can be modeled as a combination of multiplier and time integrator, the proposed method uses the camera as a set of the multiplier and LPF of the I/Q demodulator in order to observe the change in the blinking status such as phase and amplitude of the LED light. In the following, we show the proposed method by deriving the relationship between the pixel values $p[i]$ of the LED image obtained by the camera in the ith acquisition. Let the LED luminance value be $b(t)$, which blinks with phase θ and amplitude α. The pixel value $p[i]$ obtained in every frame period T_f is a value proportional to the integral of the luminance value during the exposure time. By utilizing the exposure function $e(t)$, which indicates the opening and closing of the electronic shutter, the pixel value $p[i]$ can be expressed by

$$p[i] = \int_{(i-1)T_f}^{iT_f} hb(t)e(t)dt, \tag{5}$$

where h is the proportionality coefficient between the pixel value and luminance, which depends on various factors such as the light path and the gain of the image sensor [29]. Here, we assumed that h is constant and noise in the pixel values is zero in (5). As exposure function $e(t)$ in (5) corresponds to the electronic shutter status, the exposure function is a periodic square wave function with a '1' value once per frame period T_f for a duration of exposure time T_e represented as

$$e(t) = \sum_k u_e(t - (k-1)T_f), \tag{6}$$

where

$$u_e(t) = \begin{cases} 1 & (0 \leq t \leq T_e) \\ 0 & (\text{otherwise}). \end{cases} \tag{7}$$

Fig. 2 depicts how the pixel value $p[i]$ is obtained.

Next, we compare the part enclosed by dashed lines in Fig. 2 with part in Fig. 1(a) and consider that the input signal $hb(t)$, exposure function $e(t)$, and time integrator correspond to the input signal $s(t)$, carrier signal $\cos(t)$, and LPF, respectively. Since the exposure function can only take values of 0 and 1, instead of $\cos(t)$, a square wave as shown in (6) with a duty ratio of 50%, i.e., $T_e = T_f/2$, should be used as the carrier

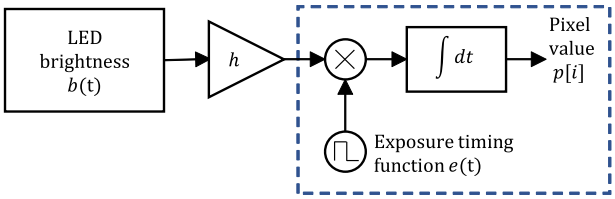

Fig. 2. Simple model from LED brightness values to camera pixel values.

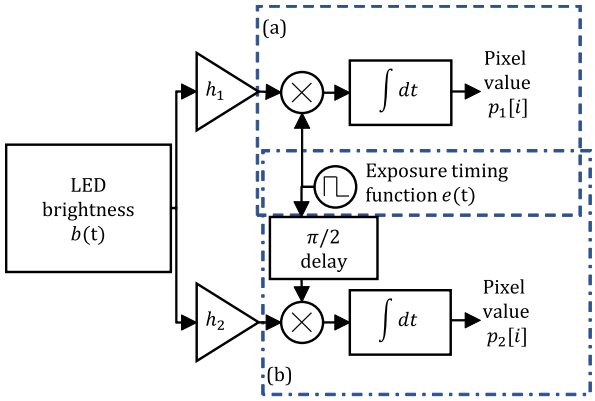

Fig. 3. Implementation model of I/Q demodulator by cameras. (a) In-phase component demodulator part, corresponding to (a) in Fig. 1. (b) Quadrature component demodulator part, corresponding to (b) in Fig. 1.

signal. As a result, the camera works as part (a) of the I/Q demodulator in Fig. 1. Next, to realize (b) in Fig. 1 with a camera, the proposed method employs an additional camera with the exposure function delayed by $\pi/2$ rad. This suggests that two cameras with the same exposure time T_{e} can be used to construct an I/Q demodulator, as shown in Fig. 3.

In the following, we derive the relationship between the pixel value and the LED blinking status in this I/Q demodulator system. In the proposed method, the relationship between the frame period T_{f} and the blinking period T_{b} is defined as $T_{\mathrm{f}} = rT_{\mathrm{b}}$, where r is the integer ratio value. For simplicity, here we assume that $T_{\mathrm{f}} = T_{\mathrm{b}}$. We define the LED blinking luminance $b(t)$ as a phase- and amplitude-modulated square wave with a duty ratio of 50% as

$$b(t) = \alpha q\left(t + T_{\mathrm{b}}\frac{\theta}{2\pi}\right) + b_m, \tag{8}$$

where α, θ, and b_m are the amplitude, phase, and luminance bias that keeps the LED luminance positive, respectively. In addition, $q(t)$ is a square wave as

$$q(t) = \sum_k u_{\mathrm{sq}}\left(t - (k-1)\,T_{\mathrm{b}}\right), \tag{9}$$

and $u_{\mathrm{sq}}(t)$ is a pulse as

$$u_{\mathrm{sq}}(t) = \begin{cases} 1 & (0 \le t \le \frac{T_{\mathrm{b}}}{2}) \\ -1 & (\text{otherwise}). \end{cases} \tag{10}$$

Note that the square wave $q(t)$ corresponds to the carrier wave of the proposed system. This LED blinking is captured by each camera that observes the in-phase and quadrature components.

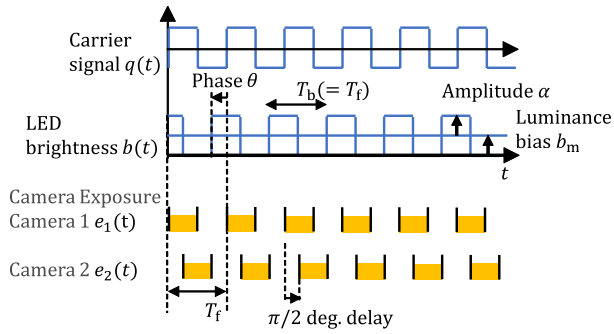

Fig. 4. Relationship between blinking and exposure of the cameras in the proposed method based on the principle of I/Q demodulator.

The exposure function $e_1(t)$ for observing the in-phase component is defined as

$$e_1(t) = \frac{1}{2}q(t) + \frac{1}{2}, \tag{11}$$

and the exposure function $e_2(t)$ for observing the quadrature component is defined as

$$e_2(t) = \frac{1}{2}q\left(t - \frac{T_{\mathrm{b}}}{4}\right) + \frac{1}{2}. \tag{12}$$

These $e_1(t)$ and $e_2(t)$ functions correspond to the in-phase local carrier $\cos(\omega_{\mathrm{c}}t)$ in (3) and quadrature local carrier $-\sin(\omega_{\mathrm{c}}t)$ in (4), respectively. We show the relationship between the LED blinking waveform and the exposure of the two cameras in Fig. 4.

By using these exposure functions, the pixel values are expressed by

$$p_1[i] = h_1 \int_{(i-1)T_{\mathrm{f}}}^{iT_{\mathrm{f}}} b(t)e_1(t)dt, \tag{13}$$

$$p_2[i] = h_2 \int_{(i-1)T_{\mathrm{f}}}^{iT_{\mathrm{f}}} b(t)e_2(t)dt, \tag{14}$$

where the coefficients h_1 and h_2 are the constants of proportionality between pixel values and LED luminance. By applying the Fourier series expansion to the square waves $b(t)$, $e_1(t)$, and $e_2(t)$ [30], we obtain

$$\begin{aligned} p_1[i] = h_1 \int_{(i-1)T_{\mathrm{f}}}^{iT_{\mathrm{f}}} & \left\{\alpha\frac{4}{\pi}\sum_{i=1}^{\infty}\frac{\sin\left((2i-1)\left(\frac{2\pi t}{T_{\mathrm{b}}}+\theta\right)\right)}{(2i-1)} + b_m\right\} \\ & \times\left\{\frac{2}{\pi}\sum_{i=1}^{\infty}\frac{\sin\left((2i-1)\left(\frac{2\pi t}{T_{\mathrm{b}}}\right)\right)}{(2i-1)} + \frac{1}{2}\right\}dt, \end{aligned} \tag{15}$$

$$\begin{aligned} p_2[i] = h_2 \int_{(i-1)T_{\mathrm{f}}}^{iT_{\mathrm{f}}} & \left\{\alpha\frac{4}{\pi}\sum_{i=1}^{\infty}\frac{\sin\left((2i-1)\left(\frac{2\pi t}{T_{\mathrm{b}}}+\theta\right)\right)}{(2i-1)} + b_m\right\} \\ & \times\left\{\frac{2}{\pi}\sum_{i=1}^{\infty}\frac{\sin\left((2i-1)\left(\frac{2\pi t}{T_{\mathrm{b}}}-\frac{\pi}{2}\right)\right)}{(2i-1)} + \frac{1}{2}\right\}dt. \end{aligned} \tag{16}$$

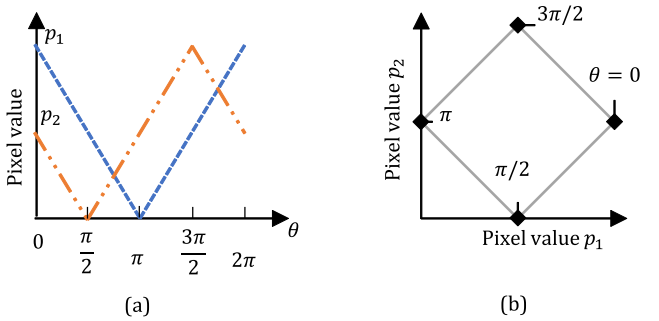

Fig. 5. (a) Relationship between pixel values. (b) Pixel value trajectory with respect to phase.

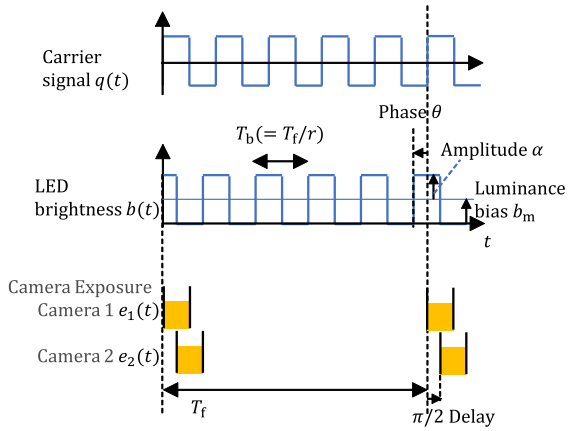

Fig. 6. Relationship between LED blinking and exposure when frames are decimated.

By simplifying (15) and (16), we obtain

$$\begin{aligned} p_1[i] &= \frac{h_1 T_f}{2}\left\{\alpha\frac{8}{\pi^2}\sum_{i=1}^{\infty}\frac{\cos\left((2i-1)\theta\right)}{(2i-1)^2}+b_m\right\} \\ &= A_1\left\{\alpha\frac{8}{\pi^2}\sum_{i=1}^{\infty}\frac{\cos\left((2i-1)\theta\right)}{(2i-1)^2}\right\}+m_1 \\ &= \begin{cases}\alpha A_1\frac{\pi/2-\theta}{\pi/2}+m_1 & (0\le\theta<\pi)\\ \alpha A_1\frac{\theta-3\pi/2}{\pi/2}+m_1 & (\text{otherwise}),\end{cases} \end{aligned} \tag{17}$$

$$\begin{aligned} p_2[i] &= \frac{h_2 T_f}{2}\left\{\alpha\frac{8}{\pi^2}\sum_{i=1}^{\infty}\frac{\cos\left((2i-1)\left(\theta+\frac{\pi}{2}\right)\right)}{(2i-1)^2}+b_m\right\} \\ &= A_2\left\{\alpha\frac{8}{\pi^2}\sum_{i=1}^{\infty}\frac{\cos\left((2i-1)\left(\theta+\frac{\pi}{2}\right)\right)}{(2i-1)^2}\right\}+m_2 \\ &= \begin{cases}\alpha A_2\frac{-\theta}{\pi/2}+m_2 & (0\le\theta<\frac{\pi}{2})\\ \alpha A_2\frac{\theta-\pi}{\pi/2}+m_2 & (\frac{\pi}{2}\le\theta<\frac{3\pi}{2})\\ \alpha A_2\frac{2\pi-\theta}{\pi/2}+m_2 & (\text{otherwise}),\end{cases} \end{aligned} \tag{18}$$

where we utilized the Fourier series expansion of triangular wave [30].

Here, we define the gain coefficient $A_1 = \frac{h_1 T_f}{2}$ and $A_2 = \frac{h_2 T_f}{2}$, and we define the pixel value offset $m_1 = \frac{h_1 T_f}{2} b_m$ and $m_2 = \frac{h_2 T_f}{2} b_m$. These parameters reflect the differences in LEDs characteristics, pixel-to-pixel output characteristics, and CMOS image sensors characteristics. We assume that these parameters are constant. From (17) and (18), it can be seen that $p_1[i]$ and $p_2[i]$ are proportional to α in amplitude and the pixel values vary in a triangular waveform with respect to θ as shown in Fig. 5(a). Plotting these two-pixel values with $p_1[i]$ on the horizontal axis and $p_2[i]$ on the vertical axis, with the amplitude fixed and the phase swept, we will obtain a rhombus-shaped trajectory as shown in Fig. 5(b). In this paper, we call this plot the pixel value trajectory. $p_1[i]$ and $p_2[i]$ correspond uniquely to the phase and amplitude, as the outputs of the I/Q demodulator, s_I and s_Q, do.

To explain the principle, we made the frame period T_f equal to the blinking period T_b. However, under this condition, it is necessary to use high-speed cameras when we employ fast blinking for flicker-free communications. To overcome this problem, we introduce frame thinning, which means that the cameras capture at only every r blink; thus, the relationship between frame period T_f and blinking period T_b is $T_f = rT_b$. Accordingly, we should set the symbol period, the interval between the phase and amplitude changes in the transmitter, equal to or greater than the frame period, so that we can estimate the phase and amplitude from the pixel values of the general-purpose camera. Note that under this condition, we should set the exposure time as $T_e = T_f/2r$ so that it remains the same as before frame thinning is introduced. Fig. 6 shows the relationship between the LED blinking and the exposure when the fast blinking is captured at the frame rate of a general-purpose camera.

B. Relationship Between Pixel Values and Phase and Amplitude

We show the equations for calculating phase θ and amplitude α under the assumption that gain coefficient A_1 and A_2 and pixel value offset m_1 and m_2 are known in advance. From (17) and (18), the pixel values p_1 and p_2 of camera 1 and camera 2 can be summarized as

$$(p_1,p_2) = \begin{cases}\left(\alpha A_1\frac{\pi/2-\theta}{\pi/2}+m_1\,,\quad -\alpha A_2\frac{\theta}{\pi/2}+m_2\right) & (0\le\theta<\pi/2)\\ \left(\alpha A_1\frac{\pi/2-\theta}{\pi/2}+m_1\,,\quad \alpha A_2\frac{\theta-\pi}{\pi/2}+m_2\right) & (\pi/2\le\theta<\pi)\\ \left(\alpha A_1\frac{\theta-3\pi/2}{\pi/2}+m_1\,,\quad \alpha A_2\frac{\theta-\pi}{\pi/2}+m_2\right) & (\pi\le\theta<3\pi/2)\\ \left(\alpha A_1\frac{\theta-3\pi/2}{\pi/2}+m_1\,,\quad \alpha A_2\frac{2\pi-\theta}{\pi/2}+m_2\right) & (3\pi/2\le\theta<2\pi).\end{cases} \tag{19}$$

Next, by modifying (19), we derive the equations for obtaining α and θ from pixel values p_1 and p_2. The normalized pixel values p_1' and p_2', whose values are between -1 and 1, are defined as

$$p_1' = (p_1 - m_1)/A_1, \tag{20}$$

$$p_2' = (p_2 - m_2)/A_2. \tag{21}$$

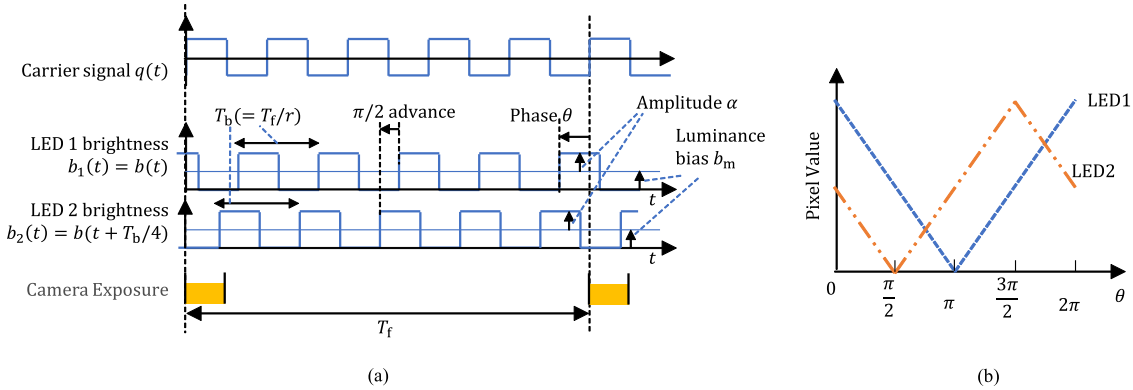

Fig. 7. (a) Relationship between blinking and exposure. (b) Relationship between pixel values and phase in the 2-LED method.

By using p'_1 and p'_2, amplitude α is expressed as

$$\alpha = |p'_1| + |p'_2|\,, \tag{22}$$

and phase θ is expressed as

$$\theta = \begin{cases} -\frac{\pi}{2}\frac{p'_1}{\alpha} + \frac{\pi}{2} & (p'_2 \le 0) \\ \frac{\pi}{2}\frac{p'_1}{\alpha} + \frac{3\pi}{2} & (p'_2 > 0). \end{cases} \tag{23}$$

Equations (22) and (23) show how the amplitude and phase can be calculated uniquely from the pixel values obtained from each of the two images captured by the camera.

The above derivation is for the noise-free case, but in actual communications, the pixel value contains noise. In such a situation, direct symbol estimation from the pixel value should be performed instead of estimation using phase and amplitude transformation as in (22) and (23). For the direct estimation, we minimize the difference between the obtained pixel value and the calculated pixel value using (19) from the phase and amplitude of all possible constellation points by assuming the noise in the pixel value is additive white Gaussian noise. Moreover, it is expected that the noise can be reduced by using the average of multiple pixel values in one image as the pixel values (sample values) for demodulation. We adopted these methods in our experiments.

C. Method Using Two LEDs

The method proposed above requires two cameras to use the I/Q demodulator mechanism. This may be a major shortcoming for some applications because it complicates the configuration of the receiver. Hence, we propose to use a configuration with two LEDs and one camera instead of one with one LED and two cameras. The two LED waveforms and camera exposure are shown in Fig. 7(a). The amplitude and luminance bias of LED 2 are the same as those of LED 1, but the phase advances $\pi/2$ rad. The light from both LEDs is captured simultaneously by one camera. The pixel values obtained by camera 2 in the two-cameras method are now obtained with the pixel values in the image of LED 2, and the pixel values for the phase are the same as when two cameras are used, as shown in Fig. 7(b). Since this correspondence relationship is also applicable to the amplitude, we can apply the phase and amplitude estimation method proposed in section III-B for this two-LED method.

D. Necessary Parameters for Communications and Solutions to Problems Caused by Asynchronous Communications in Practical use

We explained the principle of the proposed VLC method in section III-A and III-B. In those sections, we assumed that gain coefficients A_1 and A_2 and pixel value offsets m_1 and m_2 in section III-B are known. However, in the actual situation, these parameters must be obtained in advance of symbol estimation. In addition, the system is asynchronous, and there is an offset in the estimated phase which needs to be canceled out. Furthermore, symbol transitions during the exposure time cause bit errors. In this section, we describe these problems and show how they can be solved. Note that we describe the solutions using abstract ideas because the actual preamble format should be set by considering some conditions such as the environment and purpose.

1) The Pixel Value Offsets and the Gain Coefficients: As mentioned above, pixel value offsets m_1 and m_2 and gain coefficients A_1 and A_2 are necessary for demodulation. In a noise-free environment, m_1 and m_2 can be obtained by taking the pixel values when the LED lights up at $\alpha = 0$. Then, A_1 and A_2 can be obtained by taking two pairs of pixel values with different phases and known amplitudes and using (20), (21), and (22).

Since the estimation accuracy of these parameters has a significant relationship with the bit error, it is necessary to consider a more accurate estimation method by using, for example, a large number of pixel values and calculating a constant using the average.

2) The Phase Offset: Since we assume a transmitter and a receiver operate asynchronously, they cannot share the same carrier wave. This means that $q(t)$ for the blinking function shown in (8) and $q(t)$ for the exposure functions shown in (11) and (12) have different phases. The phase of a received signal is equal to the transmitted phase plus this particular phase difference. We call this phase difference the phase offset, and a receiver needs to estimate it in order to cancel it out.

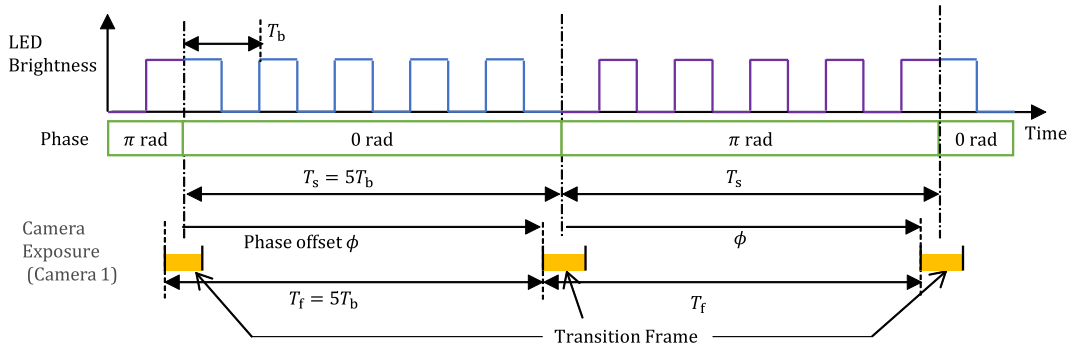

Fig. 8. Example of transition frames. If $T_s = T_f$ and once transition appears, all the following frames are transition frames.

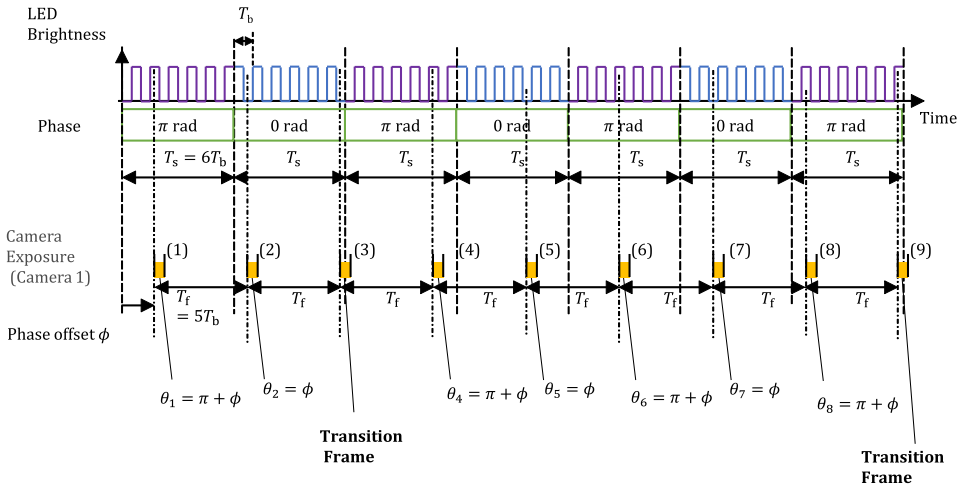

Fig. 9. Periodical appearance of transition frames under the condition $T_b : T_f : T_s = 1 : r : r + 1$. The 3 rd and 9th frames are transition frames. Symbol transition occurs in 3 rd exposure time, but correct symbol pixel values can be obtained in 2nd and 4th frames. Note that θ_i means the phase calculated from ith frame pixel values.

To estimate the phase offset, we introduce a preamble consisting of a known sequence. Note that the phase offset may vary according to time due to errors in the internal operating clock, fluctuations, etc., and those factors should be considered in designing the preamble.

3) Symbol Transitions During Exposure: Similar to existing methods [21], [29], the change in the transmitting symbol during an exposure affects the symbol estimation accuracy in our method. In this section, we describe this symbol transition problem and show how to address it. We also describe the necessary parameters for this purpose.

a) Symbol transition issue during exposure: It seems that we could achieve fast communications under a simple condition in which the frame period and symbol period match; however, this causes problems in practical use. Because of the asynchrony issue described in section III-D2, one single exposure can contain two symbols. We call a frame acquired in such exposure start timing a transition frame, and an example of this case is shown in Fig. 8. In this case, the phase and amplitude estimation method described in section III-B may give incorrect values. Moreover, all frames can be transition frames when symbol period T_s and frame period T_f are the same. For simple OOK, a solution has already been proposed [31]. However, it cannot be directly applied to our proposed principle, which uses phase and amplitude modulation; hence, an in-depth investigation is necessary.

To capture every symbol once in frames other than transition frames, we set T_s so that the period ratio is $T_b : T_f : T_s = 1 : r : r + 1$. In this setting, transition frames appear every $r + 1$ frames as shown in Fig. 9. Therefore, once a transition frame has been detected by using a preamble, the receiver can avoid the transition frames by skipping them periodically.

b) Finding transition frames in practical systems: In a practical system employing the countermeasure as described in section III-D3a, the ratio of the frame period T_f to symbol period T_s is slightly different from $r : r + 1$ due to factors such as clock errors in the transmitter and camera. In this section, we will show how to determine the transition frame using a model of exposure start timing changes by assuming that there is a constant error $\Delta T_f = T'_f - T_s \frac{r}{r+1}$ where T'_f is the actual frame period with respect to T_s. We label ΔT_f as the frame period error. Under this assumption, the exposure start timing with respect to the most recent start timing of symbol τ_i, which is shown in Fig. 10, can be calculated as

$$\tau_i = (\tau_0 + i(T_f + \Delta T_f)) \bmod T_s, \tag{24}$$

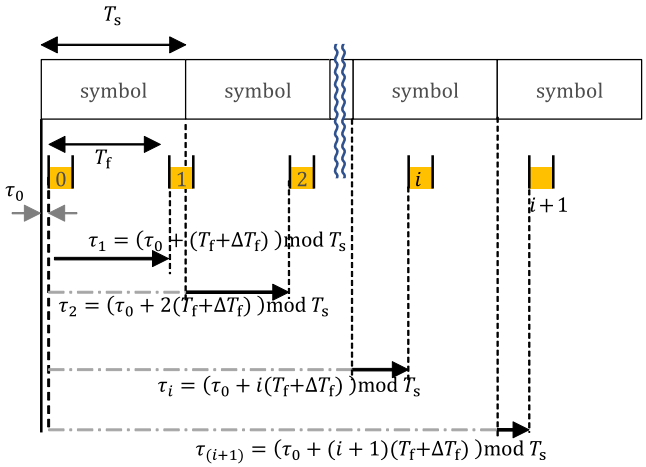

Fig. 10. Definition and example of calculation of exposure start timing τ_i.

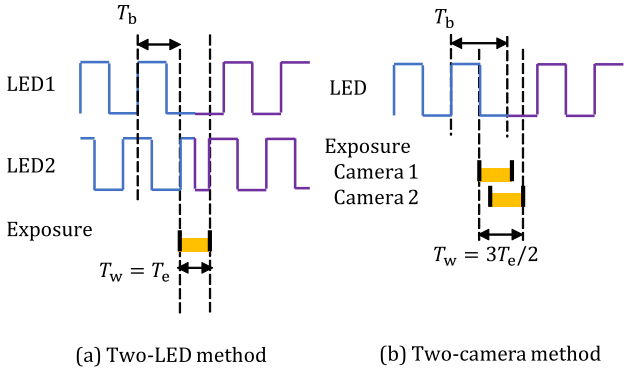

Fig. 11. Definition of observation time length T_w. A frame in which the symbol transitions during T_w should be treated as a transition frame.

where τ_0 is the initial exposure start timing. In this paper, by using the floor function $\lfloor x \rfloor$, the modulo operation "$x \bmod y$" is defined as

$$x \bmod y = x - \left\lfloor \frac{x}{y} \right\rfloor y. \tag{25}$$

To identify whether the ith frame is a transition frame or not, we introduce function $V(i, \tau_0, \Delta T_f)$, defined as

$$V(i, \tau_0, \Delta T_f) = \begin{cases} 1 & \left(\tau_i \le \left(\frac{T_b - T_w}{2}\right) \text{ or } \left(\tau_i > T_s - \frac{T_b + T_w}{2}\right)\right) \\ 0 & (\text{otherwise}), \end{cases} \tag{26}$$

where frames with $V(i, \tau_0, \Delta T_f) = 1$ and $V(i, \tau_0, \Delta T_f) = 0$ are transition frames and not transition frames, respectively. Here, as shown in Fig. 11, the observation time length T_w equals T_e for the two-LED method and $3T_e/2$ for the two-camera method.

Note that, as shown in the example in Fig. 12, if the exposure start timing of the ith frame is $0 \le \tau_i < T_b - T_w$, the same symbol will be captured in the $(i+1)$th frame. In this case, the frame which is exposed closer to the symbol transition timing is selected as the transition frame to increase the tolerance to estimation errors in the exposure start timing. The conditions in (26) already take this into account.

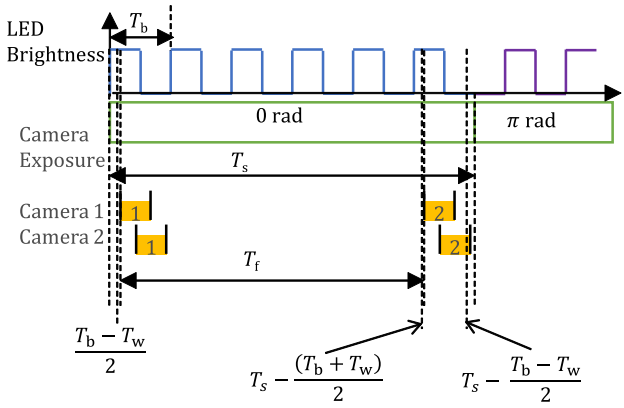

Fig. 12. The case where no symbol transition occurs in two consecutive frames. The frame exposed closer to the symbol transition timing is selected as the transition frame. In this example, the 2nd pair of frames is selected as the transition frames.

When frame period error ΔT_f exists, the phase offset also changes with time. By using the exposure start timing τ_i, the phase offset of ith frame ϕ_i can be calculated according to

$$\phi_i = \left(2\pi \frac{\tau_i}{T_b}\right) \bmod 2\pi. \tag{27}$$

IV. Experiment

To verify that the proposed principle can be used for communications, we measured the SNR-BER characteristics by carrying out experiments. In section IV-A, we explain the packet structure and how to estimate necessary parameters, which are gain coefficients A_1 and A_2, pixel value offsets m_1 and m_2, initial exposure start timing difference τ_0, and frame period error ΔT_f in the experiment. We collectively call these six parameters the demodulation parameters. In section IV-B, we describe the experimental setup and conditions.

A. Preamble Structure and Demodulation Parameters Estimation Method

In this section, we describe the preamble structure and packet format and how the demodulation parameters are estimated from the preamble.

1) Preamble and Packet Structure: In this experiment, we introduced the preamble configuration shown in Fig. 13 and used the packet configuration shown in Fig. 14. As a condition of the preamble, it is required that the average luminance perceived by the human eye does not change. Therefore, the preamble consists of no-blinking and 50% duty, 100% amplitude blinking symbols with 50% luminance bias. We set the preamble long enough to detect the transition frame at least once in the preamble. To detect the gain coefficient regardless of the phase offset, we used 0 rd., $\pi/2$ rad., π rad. and $3\pi/2$ rad. for blinking symbol phases.

2) Parameter Estimation Method: This section describes how to estimate the demodulation parameters. For accurate estimation of the demodulation parameters, we assumed that these parameters are constant in a certain number of consecutive

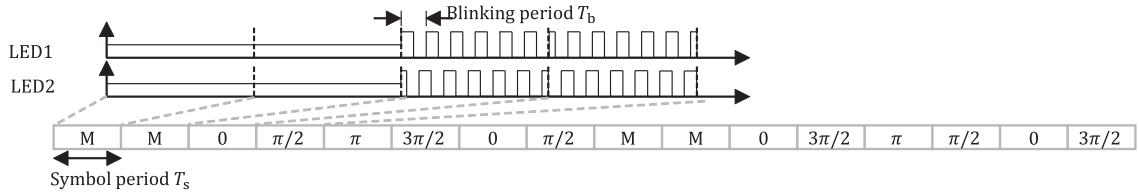

Fig. 13. Preamble configuration. 0, $\pi/2$, π, $3\pi/2$ mean blinking with this phase (unit: [rad.]) and amplitude 1. "M" means LED lights up at α=0.

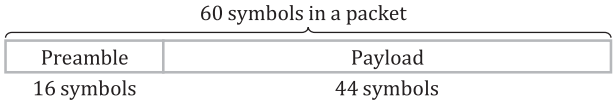

Fig. 14. Packet Configuration.

packets and estimated them for every 47 packets by using 48 preambles, including an overlapped preamble.

In this experiment, we made a model of received pixel values of the preambles and estimated them by minimizing the evaluation function $\eta(\mathbf{\Theta})$, which corresponds to the normalized square error between actual pixel values and the model, as

$$\eta\left(\mathbf{\Theta}\right)=\frac{1}{\sum_n b\left(n,\mathbf{\Theta}\right)}\sum_n b\left(n,\mathbf{\Theta}\right)\Big(\left\{p_1[n]-p_{\mathrm{m1}}\left(n,\mathbf{\Theta}\right)\right\}^2+\left\{p_2[n]-p_{\mathrm{m2}}\left(n,\mathbf{\Theta}\right)\right\}^2\Big), \tag{28}$$

where $\mathbf{\Theta}=[A_1,A_2,m_1,m_2,\tau_0,\Delta T_{\mathrm{f}}]$ is a parameter vector, n is the frame number, $p_1[n]$ and $p_2[n]$ are the pixel values observed in the nth frame, and $p_{\mathrm{m1}}(n,\mathbf{\Theta})$ and $p_{\mathrm{m2}}(n,\mathbf{\Theta})$ are the pixel values calculated by the model. The function $b(n,\mathbf{\Theta})$ is '1' if the exposure time contains only preamble symbols and is '0' otherwise. This function is used to ensure that the evaluation function contains only preambles. The demodulation process was performed by normalizing the pixel values to a minimum of 0 and a maximum of 1. Thus, parameters A_1, A_2, m_1, and m_2 take values between 0 and 1. If there is no noise, they are all 0.5. In the grid search, to account for variations due to noise, we set these ranges from 0.3 to 0.7. We also set the range of τ_0 to $\pm T_{\mathrm{f}}$ [s]. We assumed that maximum error of the frame rate was 0.02%; therefore, we set the range of ΔT_{f} to $0\pm T_{\mathrm{f}}/4500$ [s/frame] with consideration of camera and transmitter's clock unsteadiness. Since the evaluation function has many local minima, we roughly estimated the demodulation parameters by a grid search. Then, the Nelder-Mead method was used for precise estimation. The step width of the grid search was adjusted in preliminary experiments, with 0.05 step increments for parameters A_1, A_2, m_1, and m_2, $T_{\mathrm{f}}/90$ step increments for τ_0, and $T_{\mathrm{f}}/36000$ step increments for ΔT_{f}.

Using the estimated demodulation parameters, we can extract symbol information from received signals. Note that the phase offset for each frame, ϕ_i, can be calculated from τ_0 and ΔT_{f} by using (24) and (27). In this experiment, the first frame was given manually, and the last preamble in one estimation was set as the first preamble of the next estimation.

B. Experimental Setup and Conditions

We measured the SNR-BER characteristics of the proposed method by conducting experiments. The experimental system is shown in Fig. 15. The equipment used is listed in Table I. A single-board computer was used for generating transmission signals. We employed pulse width modulation (PWM) with a frequency high enough to control the LED in multilevel brightness. Two light pipes, made of acrylic rods with diffusing sanded surfaces, were used so that the luminance in the light exit plane would be uniform. We added an LED to indicate the first frame of the communications. Fig. 16 shows the transmitter structure.

We then drove two cameras by external trigger signals from a two-channel function generator and stored the captured image frames in a personal computer (PC). After that, we performed demodulation offline. The frequency was set to a frame rate of 60 Hz, and the trigger signal of camera 2 was delayed by 1/1200 seconds from camera 1. This delay corresponds to $\pi/2$ rad. delay at 300 Hz.

To control SNR in this experiment, we introduced neutral density (ND) filters to attenuate the light power of the transmitter. The combinations of ND filters used are shown in Table II. To estimate the SNRs, we captured 11 900 frames of each LED-on and LED-off for all ND filter combinations. We then calculated SNRs as

$$\mathrm{SNR}\,[\mathrm{dB}]=20\log_{10}\left(\frac{\dfrac{(\overline{p_{1\mathrm{max}}}-\overline{p_{1\mathrm{min}}})}{(s_{1\mathrm{max}}+s_{1\mathrm{min}})}+\dfrac{(\overline{p_{2\mathrm{max}}}-\overline{p_{2\mathrm{min}}})}{(s_{2\mathrm{max}}+s_{2\mathrm{min}})}}{2}\right), \tag{29}$$

where $\overline{p_{1\mathrm{max}}}$, $\overline{p_{1\mathrm{min}}}$, $\overline{p_{2\mathrm{max}}}$, $\overline{p_{2\mathrm{min}}}$, $s_{1\mathrm{max}}$, $s_{1\mathrm{min}}$, $s_{2\mathrm{max}}$, and $s_{2\mathrm{min}}$ are the average pixel values of p_1 with the LED on, that with it off, the average pixel value of p_2 with the LED on, that with it off, the pixel value standard deviation of p_1 with the LED on, that with it off, the pixel value standard deviation of p_2 with the LED on, and that with it off, respectively. In the experiments, we obtained p_1 and p_2 by averaging the pixel values in a 5×5 area around the center of the light exit plane image to eliminate characteristics variation among the pixels. This range was set manually on a LED image, and it was set only once per experimental condition.

We employed five modulation schemes—BPSK, QPSK, 8PSK, 16PSK, and 16QAM—for this experiment. The constellation map for each modulation is shown in Fig. 17. These mappings are similar to those in RF communications [27], where Gray codes are applied. The data rates were 50 bits/s in BPSK, 100 bits/s in QPSK, 150bits/s in 8PSK, and 200bits/s in both 16PSK and 16QAM. A sequence of pseudo-random symbols

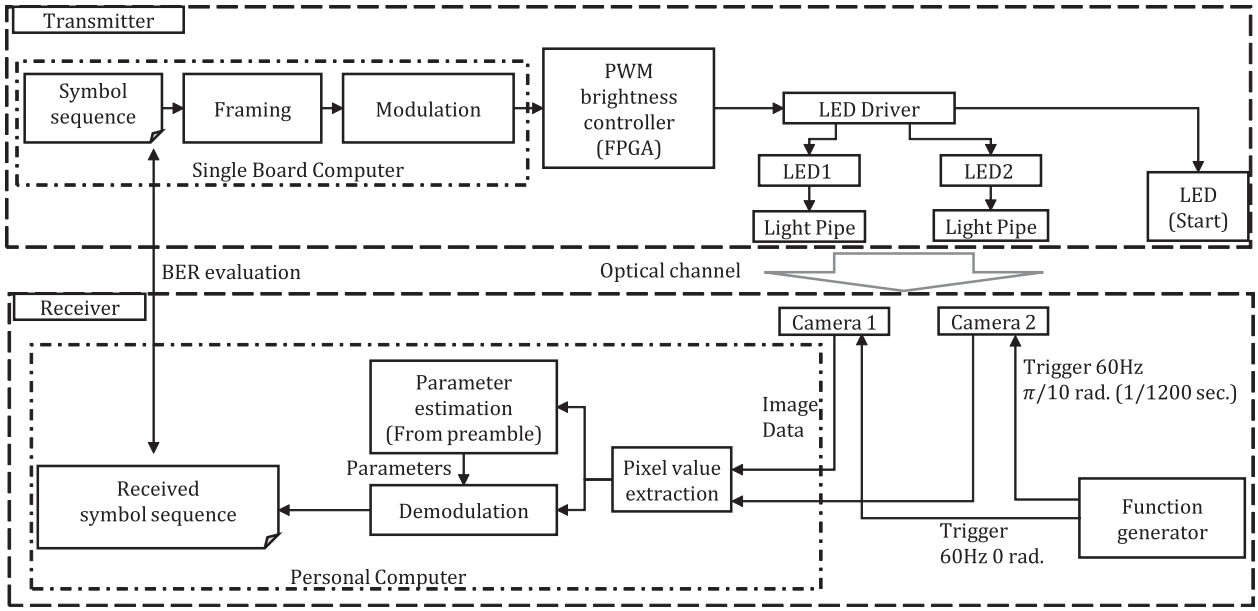

Fig. 15. System structure for communication experiments.

TABLE I
EQUIPMENT LIST

Transmitter	
Single Board Computer	Beagle Bone Black rev. C
FPGA (as PWM Brightness controller)	Digilent Cmod A7-35T
LED driver	SN74HC00
LED	Cree CLP6C-FKBCK1P1G1BB7R3R3
Light pipe	Acrylic rod with 10mm x 10mm x 100mm (Wrapped with silver tape and sanded the light exit plane by sandpaper)
ND filter	MARUMI 58mm NEO MC-ND2, MC-ND4, MC-ND8
	MARUMI 58mm DHG ND 16
	MARUMI 58mm EXUS ND 32
Receiver	
Camera	FLIR BFS-U3-04S2M
Lens	SPACECOM JHF8M-MP (with Mount adapter)
Function generator	NF Corporation WF1974
PC	eX. Computer RS5J-D81/T (Intel Core i7-6700, 8GB RAM, 500GB SSD, Ubuntu 20.04.2 LTS)
Luminance meter	Delta OHM HD2302.0 and LP471LUM2 Probe

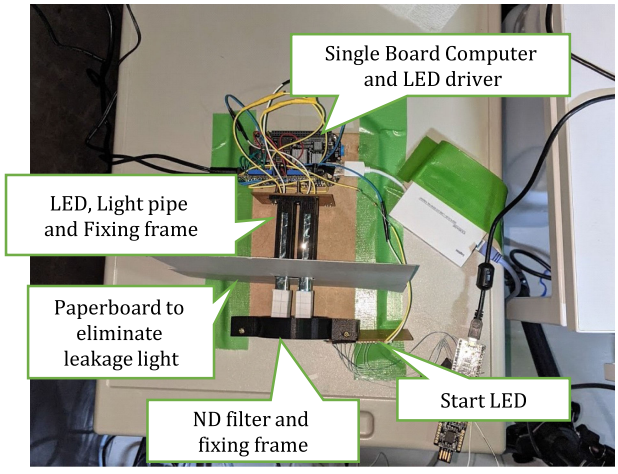

Fig. 16. Transmitter structure.

TABLE II
ND FILTER COMBINATIONS AND COMBINATION NUMBERS USED IN THE EXPERIMENTS

Combination number	ND filter combination
(1)	ND32, ND16
(2)	ND32, ND16, ND2
(3)	ND32, ND16, ND4
(4)	ND32, ND16, ND8
(5)	ND32, ND16, ND8, ND2
(6)	ND32, ND16, ND8, ND4

was used for all modulation schemes, and the number of transmitted bits was fixed to 105 600 bits for all experiments. The numbers of packets were different in the modulation scheme; 2400 in BPSK, 1200 in QPSK, 800 in 8PSK, and 600 in both 16PSK and 16QAM.

The communications distance was set at $0.97\,\mathrm{m}$. As the optical axes between the cameras and the LEDs are not aligned in

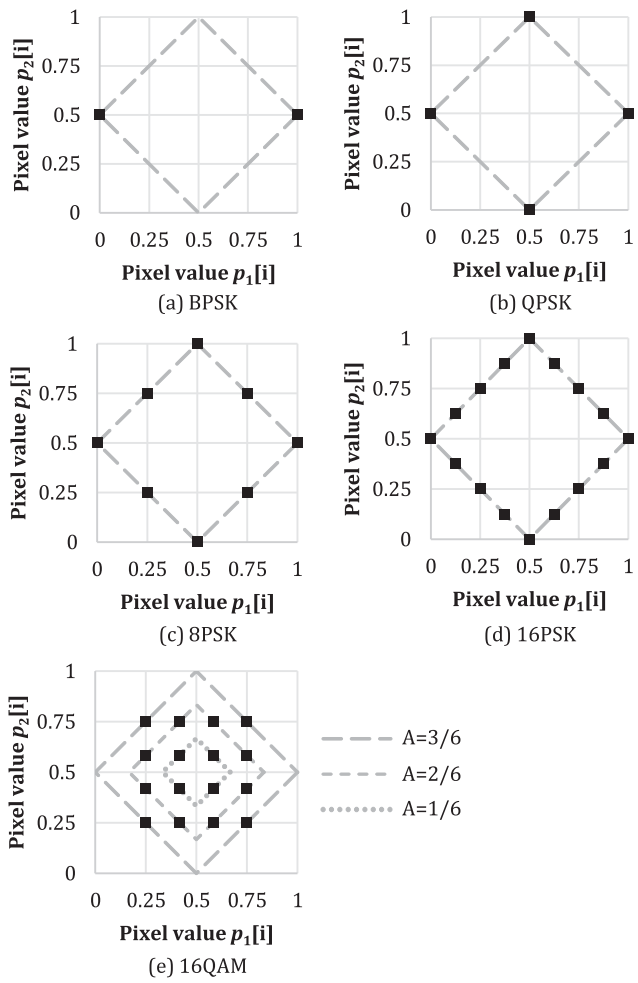

Fig. 17. Symbol assignment for each modulation. In these figures, pixel values are normalized in the range between 0 to 1.

TABLE III
KEY PARAMETERS

Symbol rate	50 symbol/sec.
LED blinking frequency	300 Hz
PWM frequency	180 kHz
Modulation scheme	BPSK, QPSK, 8PSK, 16PSK, 16QAM
Transmitted bits	105 600 bits
Frame rate	60 FPS
Communication distance (Distance from lens end to light exit plane)	0.97 m
Exposure time	1.668 ms
Camera gain	44 dB
Aperture	F8
Image sensor resolution	720 x 540
Size of the region of interest	160 x 70

practical situations, we shifted the axes as shown in Fig. 18. The experiments were carried out in a dark room. The key parameters are summarized in Table III; a photograph of the experimental setup is shown in Fig. 19.

V. RESULTS AND DISCUSSIONS

The results of BER and SNR measurements for each ND filter combination are shown in Tables IV and V. The packet error

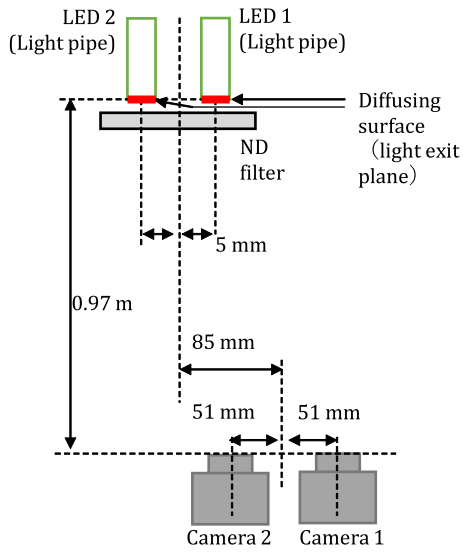

Fig. 18. Position relationship of transmitter and camera.

Fig. 19. Experimental setup.

ratios (PERs) are shown in Tables VI and VII. A graph of the SNR-BER is shown in Fig. 20. The results with the BER of less than 10^{-6}. are plotted as data with the BER of 10^{-6} in the graph. Fig. 21 plots the camera 1-camera 2 pixel values, where the estimated phase offset is around 0, which is actually in the range of $-\pi/100$ to $\pi/100$. The luminance of the transmitted light was 585.2 [cd/m^2] for LED 1 and 559.2 [cd/m^2] for LED 2 when ND filters were not applied.

Fig. 20 shows that very low BER values are achieved when the SNR is high for all modulation methods. It also shows that the two-camera and the two-LED methods have almost the same performance. In regard to the PSK modulation schemes, BPSK, which has the fewest bits per symbol, is the least sensitive to noise, and 16PSK, which has the most bits per symbol, is the most sensitive to noise. The constellations, as shown in Fig. 22, acquired the desired patterns as intended, and there was no significant distortion. This plot also shows that as the

TABLE IV
EXPERIMENTAL BER RESULTS FOR THE TWO-LED METHOD

ND combination #	BER					SNR[dB]
	BPSK	QPSK	8PSK	16PSK	16QAM	
1	0	0	0	0	9.47×10^{-6}	32.7
2	0	0	0	2.18×10^{-4}	5.02×10^{-4}	29.1
3	0	0	9.47×10^{-6}	4.51×10^{-3}	6.05×10^{-3}	25.3
4	0	0	3.30×10^{-3}	4.04×10^{-2}	5.45×10^{-2}	19.8
5	1.04×10^{-4}	3.36×10^{-3}	4.11×10^{-2}	1.15×10^{-1}	1.45×10^{-1}	14.6
6	1.43×10^{-2}	5.74×10^{-2}	1.44×10^{-1}	2.17×10^{-1}	2.68×10^{-1}	9.36

TABLE V
EXPERIMENTAL BER RESULT FOR THE TWO-CAMERA METHOD

ND combination #	BER					SNR[dB]
	BPSK	QPSK	8PSK	16PSK	16QAM	
1	0	0	0	0	9.47×10^{-6}	32.6
2	0	0	0	2.37×10^{-4}	4.92×10^{-4}	28.8
3	0	0	0	5.09×10^{-3}	7.28×10^{-3}	25.0
4	0	9.47×10^{-6}	5.48×10^{-3}	4.88×10^{-2}	6.30×10^{-2}	19.4
5	2.46×10^{-4}	4.09×10^{-3}	4.60×10^{-2}	1.20×10^{-1}	1.53×10^{-1}	14.3
6	1.84×10^{-2}	6.85×10^{-2}	1.55×10^{-1}	2.29×10^{-1}	2.78×10^{-1}	8.79

TABLE VI
EXPERIMENTAL PER RESULT FOR THE TWO-LED METHOD

ND combination #	PER				
	BPSK 2 400 packets	QPSK 1 200 packets	8PSK 800 packets	16PSK 600 packets	16QAM 600 packets
1	0	0	0	0	1.67×10^{-3}
2	0	0	0	3.67×10^{-2}	8.50×10^{-2}
3	0	0	1.25×10^{-3}	5.12×10^{-1}	6.45×10^{-1}
4	0	0	3.48×10^{-1}	9.98×10^{-1}	1.00
5	4.58×10^{-3}	2.33×10^{-1}	9.96×10^{-1}	1.00	1.00
6	4.46×10^{-1}	9.78×10^{-1}	1.00	1.00	1.00

TABLE VII
EXPERIMENTAL PER RESULT FOR THE TWO-CAMERA METHOD

ND combination #	PER				
	BPSK 2 400 packets	QPSK 1 200 packets	8PSK 800 packets	16PSK 600 packets	16QAM 600 packets
1	0	0	0	0	1.67×10^{-3}
2	0	0	0	4.00×10^{-2}	8.33×10^{-2}
3	0	0	0	5.80×10^{-1}	7.12×10^{-1}
4	0	8.33×10^{-4}	4.94×10^{-1}	1.00	1.00
5	1.08×10^{-2}	2.81×10^{-1}	9.99×10^{-1}	1.00	1.00
6	5.23×10^{-1}	9.96×10^{-1}	1.00	1.00	1.00

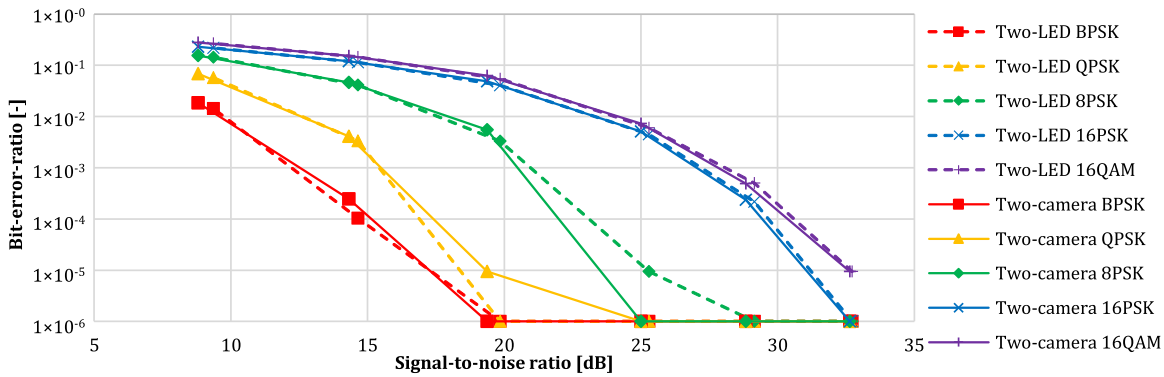

Fig. 20. SNR-BER characteristics (results with a BER below 10^{-6} are shown as 10^{-6}).

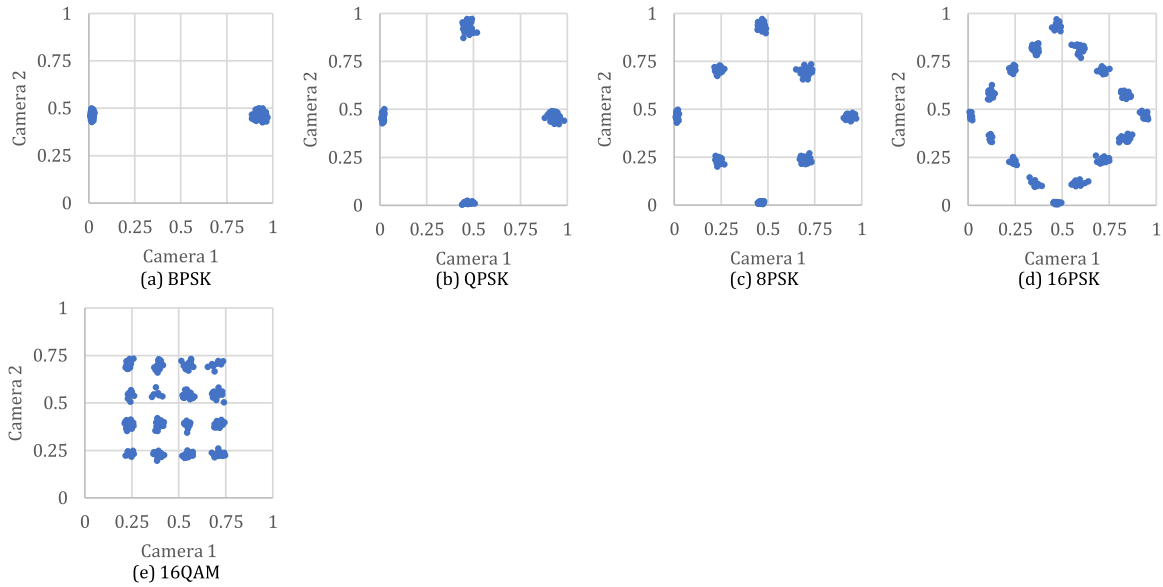

Fig. 21. 250-point camera 1-camera 2-pixel value plot when phase offset is estimated around 0 rd., which is actually in the range of $\pm\pi/100$ rad. (ND combination #1; two-camera method). Note that we excluded preamble and transition frames.

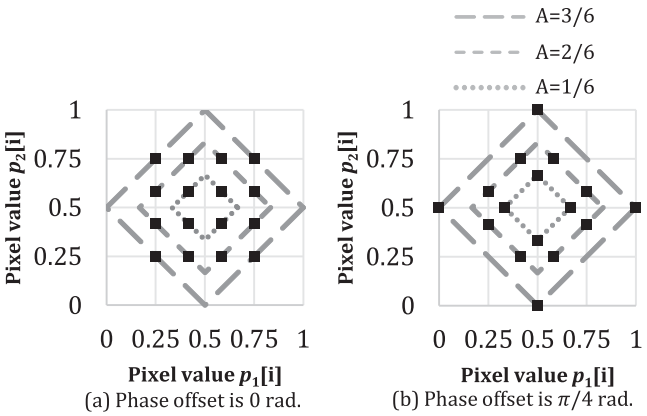

Fig. 22. Distortion of the 16QAM constellation when rotated from a phase offset of 0 rd. to $\pi/4$ rad. The constellation is distorted because the signal points move according to the rhombic-shaped trajectory. As a result, the distance between the signal points changes significantly.

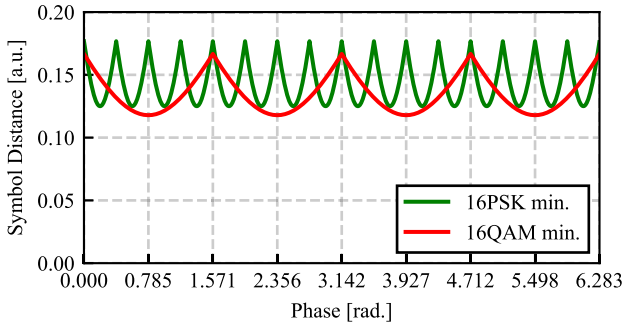

Fig. 23. Differences between 16QAM and 16PSK in theoretical minimum symbol point distance for phase offsets, where gain coefficients A_1 and A_2 are 0.5, and pixel value offsets m_1 and m_2 are 0.5. These conditions mean the minimum pixel value is 0, and the maximum is 1.

number of bits per symbol increases, the neighboring symbol points become closer to each other, and thus the margin for noise decreases.

On the other hand, the BER of 16QAM is worse than that of 16PSK, unlike in RF communications. In RF communications, as the carrier is a sinusoidal wave, the symbol points follow a circular trajectory around a certain point, and hence the distance between each symbol point is constant. In contrast, in the proposed method, which uses a square wave carrier signal, the symbol points rotate according to the rhombic-shaped trajectory, as shown in Fig. 22. This rotation on the rhombic-shaped trajectory distorts the symbol point arrangement, and the distance between the symbol points is not constant. In Fig. 23, we compare the relative minimum distances between the constellation points for 16PSK and 16QAM in the phase range of 0 to 2π. The average minimum symbol point distance for 16QAM is 0.135, and that for 16PSK is 0.143. This reversal of the distance relationship may be the reason that the BER of 16QAM is worse than that of 16PSK in our method, unlike in RF communications.

VI. Conclusion

In this paper, we have proposed a modulation and demodulation method based on the principle of the I/Q demodulator for flicker-free OCC with general-purpose low frame-rate cameras. In the proposed method, we use two cameras whose exposure start times are shifted $\pi/2$ and whose exposure time is the same as half of the blinking period so that we can obtain continuous values of the phase and the amplitude of the LED blinking at a higher frequency than the frame rate. In addition to the two-camera configuration, we showed that our proposed method can be applied to a one-camera, two-LED configuration. We conducted experiments to measure SNR-BER characteristics and verified the proposed principle in both the two-camera and two-LED configurations. In addition, in the proposed method, we found that SNR-BER characteristics differ from those of

radio communications using a general I/Q demodulator with a sinusoidal carrier wave. This difference might be due to the rhombic shape of the pixel value trajectory in the proposed method.

REFERENCES

[1] U. S. Dept. Energy, "Energy savings forecast of solidstate lighting in general illumination applications," Dec. 2019. Accessed: Jan. 27, 2022. [Online]. Available: https://www.energy.gov/sites/prod/files/2019/12/f69/2019_ssl-energy-savings-forecast.pdf

[2] P. H. Pathak, X. Feng, P. Hu, and P. Mohapatra, "Visible light communication, networking, and sensing: A survey, potential and challenges," *IEEE Commun. Surv. Tut.*, vol. 17, no. 4, pp. 2047–2077, Oct.–Dec. 2015.

[3] M. Akanegawa, Y. Tanaka, and M. Nakagawa, "Basic study on traffic information system using LED traffic lights," *IEEE Trans. Intell. Transp. Syst.*, vol. 2, no. 4, pp. 197–203, Dec. 2001.

[4] T. Komine and M. Nakagawa, "Fundamental analysis for visible-light communication system using LED lights," *IEEE Trans. Consum. Electron.*, vol. 50, no. 1, pp. 100–107, Feb. 2004.

[5] D. Tsonev *et al.*, "A 3-Gb/s single-LED OFDM-based wireless VLC link using a gallium nitride μled," *IEEE Photon. Technol. Lett.*, vol. 26, no. 7, pp. 637–640, Apr. 2014.

[6] T. Nguyen, A. Islam, T. Yamazato, and Y. M. Jang, "Technical issues on IEEE 802.15.7 m image sensor communication standardization," *IEEE Commun. Mag.*, vol. 56, no. 2, pp. 213–218, Feb. 2018.

[7] T. Yamazato *et al.*, "Image-sensor-based visible light communication for automotive applications," *IEEE Commun. Mag.*, vol. 52, no. 7, pp. 88–97, Jul. 2014.

[8] P. Luo, M. Zhang, Z. Ghassemlooy, S. Zvanovec, S. Feng, and P. Zhang, "Undersampled-based modulation schemes for optical camera communications," *IEEE Commun. Mag.*, vol. 56, no. 2, pp. 204–212, Feb. 2018.

[9] C. S. Herrmann, "Human EEG responses to 1-100 Hz flicker: Resonance phenomena in visual cortex and their potential correlation to cognitive phenomena," *Exp. Brain Res.*, vol. 137, no. 3-4, pp. 346–353, 2001.

[10] C. Danakis, M. Afgani, G. Povey, I. Underwood, and H. Haas, "Using a CMOS camera sensor for visible light communication," in *Proc. IEEE Globecom Workshops*, 2012, pp. 1244–1248.

[11] Y. Liu, "Decoding mobile-phone image sensor rolling shutter effect for visible light communications," *Opt. Eng.*, vol. 55, no. 1, pp. 1–6, 2016.

[12] C.-W. Chow, C.-Y. Chen, and S.-H. Chen, "Enhancement of signal performance in LED visible light communications using mobile phone camera," *IEEE Photon. J.*, vol. 7, no. 5, 2015, Art. no. 7903607.

[13] V. P. Rachim and W.-Y. Chung, "Multilevel intensity-modulation for rolling shutter-based optical camera communication," *IEEE Photon. Technol. Lett.*, vol. 30, no. 10, pp. 903–906, May 2018.

[14] M. A. Atta and A. Bermak, "A 160 m visible light communication link using hybrid undersampled phase-frequency shift on-off keying and CMOS image sensor," *Opt. Exp.*, vol. 27, no. 3, pp. 2478–2487, Feb. 2019.

[15] R. D. Roberts, "A MIMO protocol for camera communications (CamCom) using undersampled frequency shift ON-OFF keying (UFSOOK)," in *Proc. IEEE Globecom Workshops*, 2013, pp. 1052–1057.

[16] P. Luo, Z. Ghassemlooy, H. Le Minh, X. Tang, and H. M. Tsai, "Undersampled phase shift ON-OFF keying for camera communication," in *Proc. 6th Int. Conf. Wireless Commun. Signal Process.*, 2014, pp. 1–6.

[17] P. Luo *et al.*, "Experimental demonstration of RGB LED-based optical camera communications," *IEEE Photon. J.*, vol. 7, no. 5, Oct. 2015, Art. no. 7904212.

[18] T. Nguyen, A. Islam, and Y. M. Jang, "Region-of-interest signaling vehicular system using optical camera communications," *IEEE Photon. J.*, vol. 9, no. 1, Feb. 2017, Art. no. 7900720.

[19] N. Liu, J. Cheng, and J. F. Holzman, "Undersampled differential phase shift ON-OFF keying for optical camera communications," *J. Commun. Inf. Netw.*, vol. 2, no. 4, pp. 47–56, Dec. 2017.

[20] P. Luo, Z. Ghassemlooy, H. L. Minh, H.-M. Tsai, and X. Tang, "Undersampled-PAM with subcarrier modulation for camera communications," in *Proc. Opto- Electron. Commun. Conf.*, 2015, pp. 1–3.

[21] S. A. I. Alfarozi, K. Pasupa, H. Hashizume, K. Woraratpanya, and M. Sugimoto, "Square wave quadrature amplitude modulation for visible light communication using image sensor," *IEEE Access*, vol. 7, pp. 94806–94821, 2019.

[22] A. Bravo and F. Cruz-Roldan, "Digital quadrature demodulator with four phases mixing for digital radio receivers," *IEEE Trans. Circuits Syst. II: Analog Digit. Signal Process.*, vol. 50, no. 12, pp. 1011–1015, Dec. 2003.

[23] W. Kihara and T. Yendo, "A communication method for asynchronous visible light communication based image sensor," in *Proc. IEEE Globecom Workshops*, 2017, pp. 1–6.

[24] W. Kihara, T. Yendo, Y. Shiraki, T. G. Sato, and T. Moriya, "PSK modulation in camera based VLC for receiving from distributed transmitters," in *Proc. Int. Conf. Exhib. Visible Light Commun.*, 2018, pp. 1–6.

[25] "Kookmin University comments to TCD 15-492r2: Flickering consideration for OWC," Jul. 2015. Accessed: Nov. 28, 2021. [Online]. Available: https://mentor.ieee.org/802.15/dcn/15/15-15-0575-01-007a-kookmin-university-comments-to-tcd-15-492r2-flickering-consideration-for-owc.ppt

[26] T. Nguyen, A. Islam, T. Hossan, and Y. M. Jang, "Current status and performance analysis of optical camera communication technologies for 5G networks," *IEEE Access*, vol. 5, pp. 4574–4594, 2017.

[27] A. Goldsmith, *Wireless Communications, Ser. Cambridge Core*. Cambridge, U.K.: Cambridge Univ. Press, 2005.

[28] S. A. Bassam, S. Boumaiza, and F. M. Ghannouchi, "Block-wise estimation of and compensation for I/Q imbalance in direct-conversion transmitters," *IEEE Trans. Signal Process.*, vol. 57, no. 12, pp. 4970–4973, Dec. 2009.

[29] W. Mao and J. M. Kahn, "Free-space heterochronous imaging reception of multiple optical signals," *IEEE Trans. Commun.*, vol. 52, no. 2, pp. 269–279, Feb. 2004.

[30] M. Cartwright, *Fourier Methods for Mathematicians, Scientists and Engineers*. Chichester, West Sussex, U.K.: Ellis Horwood, 1990.

[31] Y. Shiraki *et al.*, "A demodulation method using a Gaussian mixture model for unsynchronous optical camera communication with on-off keying," *J. Lightw. Technol.*, vol. 39, no. 6, pp. 1742–1755, 2021.